ARTICLE OPEN

Check for updates

ISCA2 inhibition decreases HIF and induces ferroptosis in clear cell renal carcinoma

Yangsook Song Green[1], Maria C. Ferreira dos Santos[2], Daniel G. Fuja[1], Ethan C. Reichert[1], Alexandre R. Campos[3], Sophie J. Cowman[1], Karen Acuña Pilarte[1], Jessica Kohan[4], Sheryl R. Tripp[4], Elizabeth A. Leibold[1], Deepika Sirohi[4,5], Neeraj Agarwal[5], Xiaohui Liu[2] and Mei Yee Koh[1,2,5]✉

Clear cell renal cell carcinoma (ccRCC), the most common form of kidney cancer, is typically initiated by inactivation of the von Hippel Lindau (*VHL)* gene, which results in the constitutive activation of the hypoxia inducible factors, HIF-1α and HIF-2α. Using a high throughput screen, we identify novel compounds that decrease HIF-1/2α levels and induce ferroptosis by targeting Iron Sulfur Cluster Assembly 2 (ISCA2), a component of the late mitochondrial Iron Sulfur Cluster (L-ISC) assembly complex. ISCA2 inhibition either pharmacologically or using siRNA decreases HIF-2α protein levels by blocking iron-responsive element (IRE)-dependent translation, and at higher concentrations, also decreases HIF-1α translation through unknown mechanisms. Additionally, ISCA2 inhibition triggers the iron starvation response, resulting in iron/metals overload and death via ferroptosis. ISCA2 levels are decreased in ccRCC compared to normal kidney, and decreased ISCA2 levels are associated with pVHL loss and with sensitivity to ferroptosis induced by ISCA2 inhibition. Strikingly, pharmacological inhibition of ISCA2 using an orally available ISCA2 inhibitor significantly reduced ccRCC xenograft growth in vivo, decreased HIF-α levels and increased lipid peroxidation, suggesting increased ferroptosis in vivo. Thus, the targeting of ISCA2 may be a promising therapeutic strategy to inhibit HIF-1/2α and to induce ferroptosis in pVHL deficient cells.

Oncogene (2022) 41:4709–4723; https://doi.org/10.1038/s41388-022-02460-1

INTRODUCTION

Clear cell renal cell carcinoma (ccRCC) is highly refractory to standard chemotherapy and radiation and is one of the most common and aggressive subtypes of kidney cancer. Patients with advanced or metastatic tumors (30% of patients) have a 5-year survival rate of just 13% [1]. The etiology of ccRCC is uniquely linked to loss of the von Hippel Lindau (*VHL*) tumor suppressor gene, resulting in the pseudo-hypoxic activation of the hypoxia-inducible factors, (HIF)-1α and HIF-2α [2–4]. The VHL protein (pVHL) is the substrate recognition component of the E3 ligase complex that targets HIF-1α and HIF-2α subunits for proteasomal degradation under aerobic conditions [5]. Under hypoxic conditions, or in the presence of pVHL loss-of-function mutations, HIF-1α and HIF-2α are stabilized, and enter the nucleus where they heterodimerize with HIF-1β, forming the HIF-1 or HIF-2 transcriptional complexes, respectively. The HIF heterodimers bind to conserved hypoxia response elements (HREs) within regulatory regions of target genes to activate transcription of hundreds of genes critical for the adaptation to hypoxia, and for tumor progression, such as those promoting aerobic glycolysis, angiogenesis, and metastasis [6, 7]. In addition to canonical HRE-mediated transcription requiring hetero-dimerization with HIF-1β, the HIF-1α and HIF-2α subunits differentially modulate cellular signaling pathways through interaction with proteins that do not contain PAS domains, including the tumor suppressor protein p53, the c-MYC proto-oncogene, β-catenin and the Notch intracellular domain [8–13].

HIF-1 versus HIF-2-specific activation is determined, at least in part, by factors within the tumor microenvironment such as intensity and duration of hypoxia, as well as cell-type-specific pathway activation within both tumor cells and those of the complex tumor microenvironment [14–16]. Consequently, although the HIFs share many transcriptional targets, they also regulate non-overlapping genes: For example, anerobic glycolysis is predominantly HIF-1 controlled, whereas erythropoietin *(EPO)* synthesis and iron uptake in the gut have emerged as primarily HIF-2-regulated processes [17–21]. Indeed, HIF-2α plays a non-redundant role in iron regulation and is additionally regulated at the translational level by an RNA stem-loop element known as an iron-responsive element (IRE), within the 5′ untranslated region (UTR) of the HIF-2α transcript [22]. Under conditions of iron depletion, iron regulatory proteins (IRP1 and IRP2) bind to IREs within 5′ or 3′ UTRs of transcripts resulting in translational repression and transcript stabilization respectively. The IRPs coordinate the cellular response to iron starvation by decreasing iron storage and increasing iron uptake such as through down-regulation of the central iron storage molecule, ferritin (FTH1; 5′ IRE) and upregulation of the major mediator of cellular iron

[1]University of Utah, Salt Lake City, UT 84112, USA. [2]Kuda Therapeutics, Inc, Salt Lake City, UT 84103, USA. [3]Sanford Burnham Prebys Medical Discovery Institute, La Jolla, CA 92037, USA. [4]ARUP Institute for Clinical and Experimental Pathology, Salt Lake City, UT 84108, USA. [5]Huntsman Cancer Institute, University of Utah, Salt Lake City, UT 84112, USA. ✉email: mei.koh@utah.edu

Received: 11 April 2022 Revised: 23 August 2022 Accepted: 26 August 2022
Published online: 12 September 2022

uptake, transferrin receptor (TFRC; 3′IRE) respectively. In this regard, binding of IRP1 to the 5′IRE of HIF-2α mediates HIF-2α translational repression during conditions of iron (or Fe-S cluster) insufficiency to limit erythropoiesis [22].

HIF-2α has been proposed to play a dominant driving role over HIF-1α in ccRCC [23, 24]. The HIF-2 bias observed in ccRCC may be due to the increased potency of HIF-2α compared to HIF-1α in promoting pro-tumorigenic factors such as Cyclin D1, TGF-α and VEGFA [23, 25]. HIF-2α has also been implicated in ccRCC metastasis through activation of CXCR4, and in driving the transcription of stem cell factors *OCT-3/4* and *SOX2*, which promote an undifferentiated, more aggressive phenotype [26–31]. The first-in-class HIF-2α selective inhibitor, belzutifan, which blocks the heterodimerization of HIF-2α with HIF-1β, shows promising single-agent activity in heavily pre-treated patients with advanced ccRCC, and was recently approved for the treatment of cancers associated with VHL disease [32, 33]. Although these studies support a tumor-promoting role for HIF-2α in ccRCC, recent data suggest that HIF-1α may also contribute to ccRCC progression in the context of the complex tumor microenvironment [15, 34, 35]. This suggests that the targeting of HIF-1α, in addition to HIF-2α may provide additional therapeutic benefit in ccRCC.

Here, we describe the results of a high-throughput screen for selective inhibitors for HIF-2α that reveal a series of small molecules that decrease HIF-2α protein, and at higher concentrations, also HIF-1α. These compounds mediate their effects by inhibiting the function of iron sulfur cluster assembly 2 (ISCA2) which blocks IRE-dependent HIF-2α translation and inhibits HIF-1α translation through unknown mechanisms. Significantly, we show that these ISCA2 inhibitors trigger the iron starvation response resulting in the accumulation of iron (and of other transition metals) that induce death via ferroptosis both in vitro and in vivo. Ferroptosis is a form of necrotic cell death associated with iron-dependent oxidation of phospholipid membranes, which causes defects within the plasma and mitochondrial membranes resulting in cell death [36, 37]. The induction of ferroptosis is a promising therapeutic strategy for cancer, particularly those with clear cell morphology such as ccRCC [38]. A number of potent ferroptosis inducers that trigger ferroptosis in vitro (e.g. erastin, RSL3) have been described but these are unsuitable as clinical candidates, at least in part, due to their unfavorable drug-like properties that make them unsuitable for oral administration [39, 40]. Thus, we describe a novel role of ISCA2 in HIF and iron regulation and highlight its value as a potential therapeutic target in ccRCC for the dual inhibition of HIF-α and the induction of ferroptosis.

RESULTS

A high-throughput screen for HIF-2α inhibitors identify compounds that decrease HIF-2α translation

To identify inhibitors of HIF-2α, we performed a high throughput screening campaign of the 360,000 compound NIH Molecular Libraries Probe Production Centers Network (MLPCN) using a hypoxia-responsive element (HRE)-luciferase based screen in 786-0 RCC cells (express HIF-2α exclusively), followed by a counter-screen using deferoxamine-treated MIA-PaCa2 pancreatic cancer cells (express HIF-1α exclusively). Screen flow chart and HIF-α dependency of HRE-luciferase activity in 786-0 HRE and MIAPaCA-2 HRE cells are shown in Fig. 1A–C respectively. In the initial screen, 2626 compounds were identified as primary actives in 786-0 HRE cells. These compounds reduced HIF-2α activity by at least 40% (Z′ average = 0.84, Signal/background ratio 40 = 76.8). Promiscuous compounds were filtered, reducing the number of actives to 1927. Of these, 982 hits were reconfirmed using fresh powder. Of the confirmed hits, 209 compounds showed ≤50% inhibition of reporter activity in the HIF-1α selectivity assay in the MIAPaCA-2 HRE cells, suggesting that these hits selectively inhibited HIF-2α compared to HIF-1α. Retesting with fresh powder and eliminating non-actives or non-selective inhibitors of luciferase, followed by structure activity relationship (SAR) studies identified compound #1 and its more potent derivative, compound #25 that decreased HIF-2α activity and protein in a variety of cell lines (Fig. 1D–G, Supplementary Data S1A). These compounds also decreased HIF-1α levels at higher concentrations or treatment durations (Fig. 1F, G). Treatment with the proteasomal inhibitor, MG132 did not prevent the decrease in HIF-1/2α mediated by #1 or #25 (Fig. 1G), suggesting that these compounds do not promote proteasomal degradation of HIF-1/2α. Furthermore, although treatment of cells with #1 or #25 resulted in a dose-dependent decrease in the transcription of HIF-2α target genes *VEGFA* and *POU5F1*, neither compound significantly affected levels of HIF-2α (*EPAS1*) transcript (Figs. 1H, S1B), indicating that these compounds do not inhibit HIF-2α transcription. Indeed, we found that #1 and #25 inhibited the production of luciferase driven by the HIF-2α IRE (IRE-Luc) (Figs. 1I, S1C) suggesting that these compounds block IRE-dependent translation of HIF-2α [22]. The decrease in HIF-2α translation was confirmed by decreased puromycin incorporation into immunoprecipitated HIF-2α in hypoxic ACHN cells treated with #1 using the SUnSET assay (S1D) [41]. In addition to decreasing HIF1/2α levels, we also noted dose-dependent increases in IRP2 and TFRC and decreased FTH after treatment with #1 or #25, which together indicate the triggering of the iron starvation response, which would be consistent with the IRP1/IRE mediated translational inhibition of HIF-2α that we have observed (Fig. 1E, F). Thus, using a high-throughput screening campaign, we have identified a series of small molecules that decrease HIF-2α by inhibiting IRE-dependent translation, and that also inhibit HIF-1α at higher concentrations/treatment durations.

HIF-α inhibitors target ISCA2 and trigger the iron starvation response

To identify the molecular target of #1 and #25, we used the drug affinity responsive target stability (DARTS) assay, which is based on the principle that the binding of a small molecule to its target renders the latter protease resistant [42]. We used 2D-LC-MS/MS to identify peptides differentially degraded by pronase (a mixture of proteases) in the absence or presence of #1 (100 µM) using hypoxic ACHN cell lysates (Fig. 2A). From more than 2000 unique proteins detected, we confirmed ISCA2 as the most likely molecular target for #1 via both 2D-LCMS/MS and western blotting (Fig. 2B). Indeed, pre-treatment with #1 prior to pronase incubation increased the amount of ISCA2 detected by 2D-LC-MS/MS by almost 5-fold, and this increase in ISCA2 levels were detectable via western blotting (Fig. 2B), suggesting that #1 protects ISCA2 from pronase-mediated degradation. ISCA2 was further validated as the likely molecular target of these compounds using thermal shift studies using recombinant ISCA2 wherein treatment with either #1 or #25 induced significant increases in the melting temperature of ISCA2 compared to DMSO alone (Fig. 2B, C). Additionally, siRNA knockdown of ISCA2 dramatically reduced both HIF-1α and HIF-2α protein levels, confirming ISCA2 as the likely molecular target of these compounds (Fig. 2D). Furthermore, treatment with #1 and #25 markedly reduced levels of ISCA2 in 786-0 and RCC10 cells (Fig. 1E–G). However, unlike treatment with #1 and #25 which induced IRP2 and TFRC, ISCA2 siRNA markedly reduced the levels of these proteins (Fig. 2D), which may be due to the extended duration of ISCA2 siRNA transfection required to reduce ISCA2 protein levels (6 days), compared to the relatively short period of drug treatment (24 or 72 h). Regardless of these differences, we identified a significant increase in iron and other transition metals when cells were treatment with compound #1 or #25 or transfected with ISCA2 siRNA (Figs. 2E–G, S2A–C). Thus, the data show that these compounds decrease HIF-1/2α levels and induce iron and metals accumulation by targeting ISCA2.

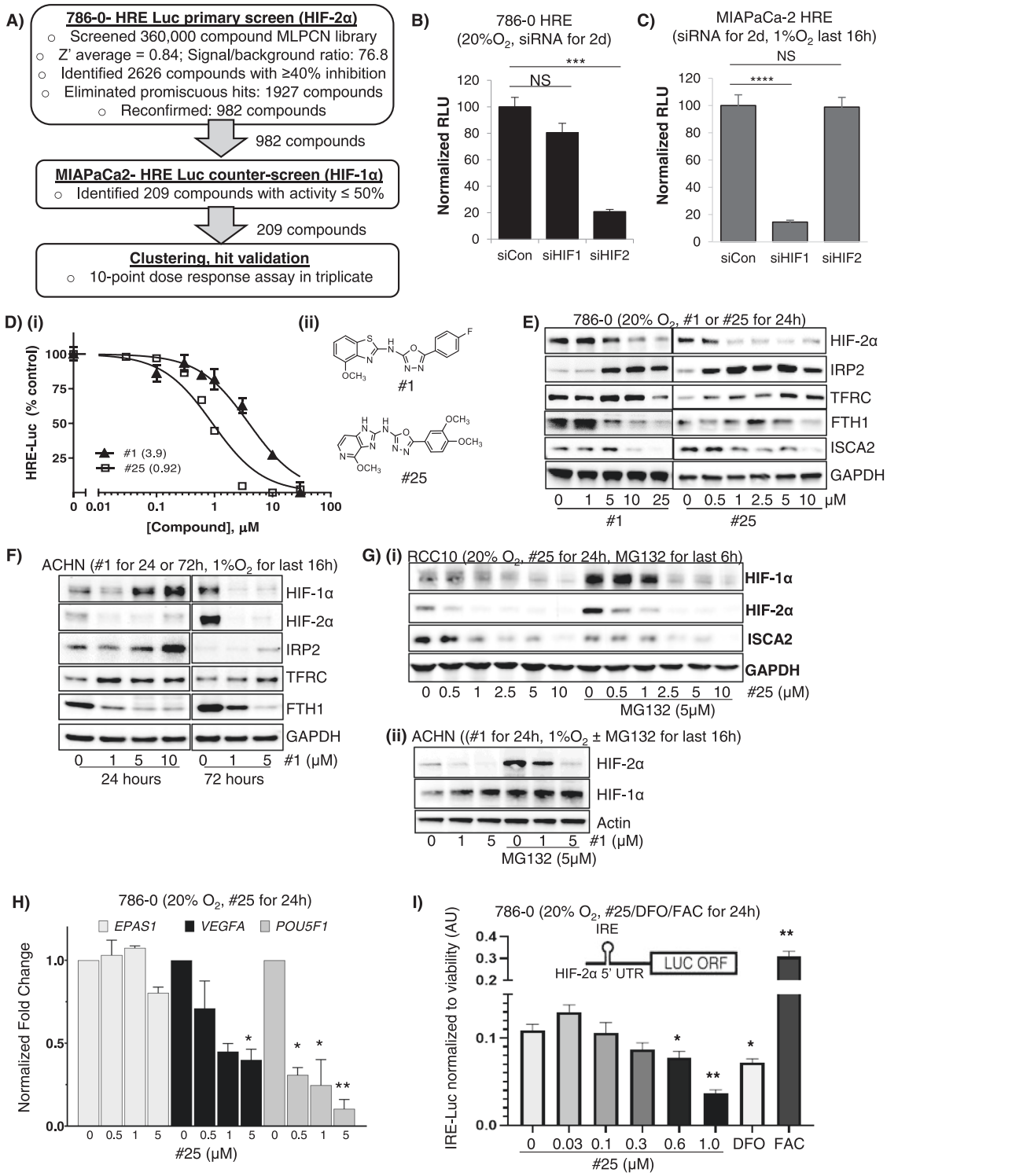

Fig. 1 Identification and characterization of novel HIF-2α selective inhibitors. A Screening flow-chart for the identification of selective small molecule inhibitors of HIF-2α. **B**, **C** Validation of HIF-1α or HIF-2α dependency of a Hypoxia Responsive Element (HRE)-driven luciferase reporter construct stably expressed in (**B**) 786-0 or (**C**) MIAPaCa-2 cells. **D** (i) 786-0 HRE-Luciferase dose-response assays of indicated compounds (24-hour treatment) with IC_{50} values (μM) indicated in brackets; (ii) Chemical structures of compounds used in the study. **E** Western blots showing effects of treatment with #1 or #25 on levels of HIF-2α and other proteins in 786-0 cells in normoxia (20% O_2). **F** Effects of 24- or 72-hours' treatment with #1 in ACHN cells (exposed to hypoxia or 1% O_2 for the final 24 h). **G** Effects of treatment of, (i) RCC10 cells with #25 ± proteasomal inhibitor, MG132 (5 μM 24 h, 20% O_2), or of (ii) hypoxic ACHN cells with #1 ± MG132 (24 h, 1% O_2) on HIF-1α and HIF-2α. **H** Quantitative RT-PCR showing effects of #25 on the transcription of *HIF2A* (*EPAS1*) and HIF-2 target genes *VEGFA* and *OCT-3/4* (*POU5F1*). **I** Effect of #25 treatment on luciferase activity driven by a HIF-2α Iron-Responsive Element (IRE)-luciferase reporter construct stably expressed in 786-0 cells. The iron chelator, deferoxamine (DFO; 50 μM), and iron donor, ferric acetylcysteine (FAC; 25 μM) were used to confirm responsiveness of the reporter to iron perturbation. All data shown are representative of at least 2 independent experiments and show the mean ± SEM. *$p < 0.05$; **$p < 0.01$.

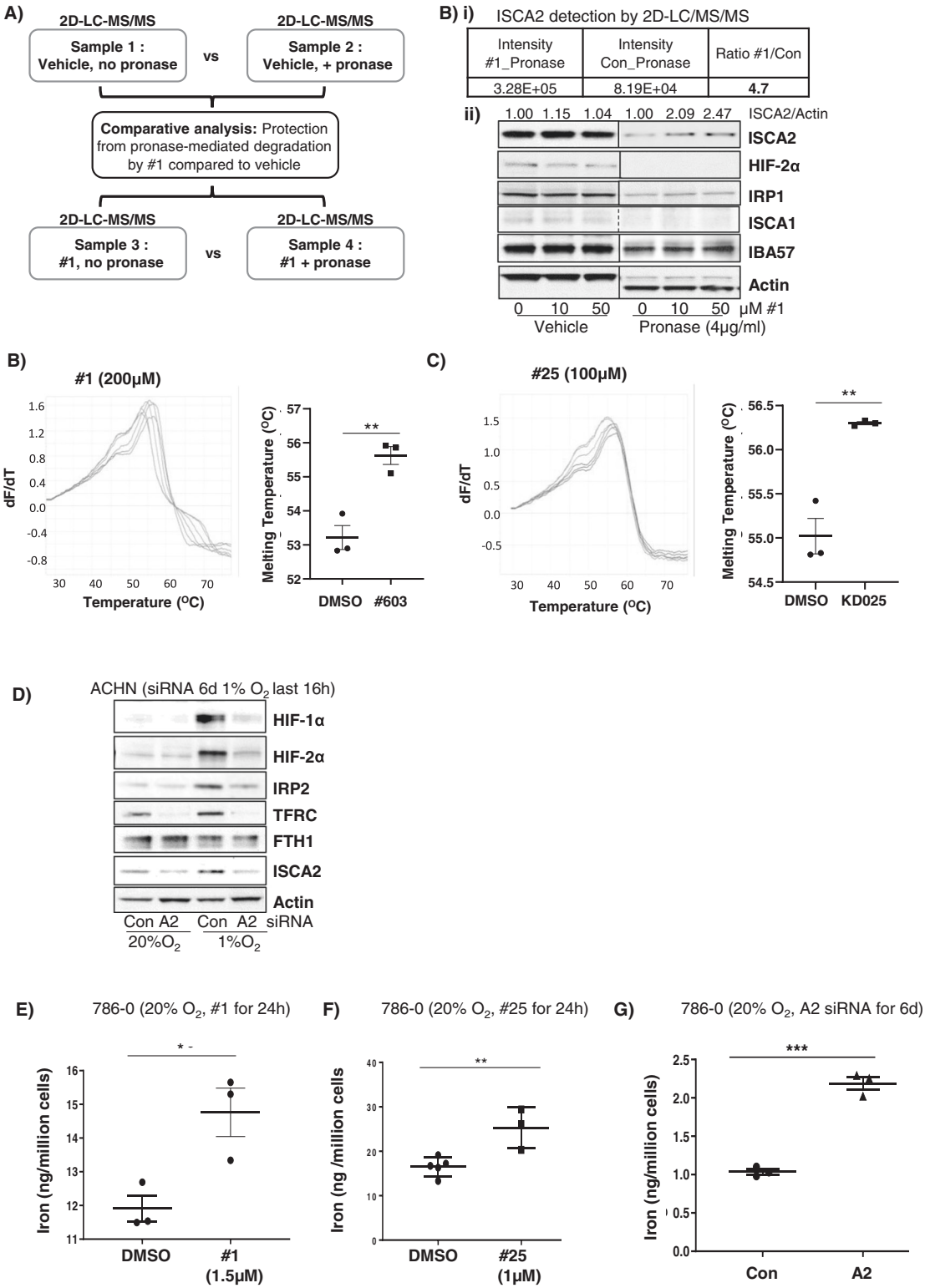

Fig. 2 ISCA2 is the molecular target of HIF-α inhibitors. A Schematic showing sample preparation workflow for DARTS assay. Lysates from ACHN cells that were exposed to 1% O_2 for 16 h were divided into 4 equal samples and subjected to indicated treatments. **B** (i) Mass spectrometry data from DARTS assay indicating intensity of ISCA2 fragments in cell lysates treated with Pronase together with #1 or DMSO (Con); (ii) Western blot showing effects of control or Pronase treatment in ACHN cell lysates treated with indicated concentrations of #1. Densitometric analysis of ISCA2 band intensities normalized to actin is shown above blots. **B**, **C** Thermal shift assays showing effects of incubation of recombinant ISCA2 (4 μg) with (**B**) DMSO (green) or 200 μM #1 (magenta), or (**C**) DMSO (green) or 100 μM #25 (red). Quantitation of ISCA2 melting temperatures are shown inset (mean ± SEM). **D** Effects of transfections with non-targeting (Con) or ISCA2 (A2) siRNA on indicated proteins in hypoxic ACHN cells. Knockdown was performed using two consecutive siRNA transfections over 72 h each. **E**–**G** Iron content of 786-0 cells treated with (**E**) #1, (**F**) #25, for 24 h; or (**G**) transfected with siCon or siISCA2 (6 days) as determined using ICP-MS.

ISCA2 inhibition affects HIF and iron sensing independent of its role in the mitochondrial iron sulfur cluster assembly complex

ISCA2, together with ISCA1 and IBA57 (Iron-Sulfur Cluster Assembly Factor for Biotin Synthase-And Aconitase-Like Mitochondrial proteins) is a component of the late mitochondrial Iron-Sulfur Cluster Assembly (L-ISC) complex, which regulates the maturation of mitochondrial iron-sulfur [4Fe-4S] proteins including respiratory chain complexes I and II, mitochondrial aconitase and lipoic acid synthase [43–46]. A robust readout of mitochondrial [4Fe-4S] function is the mitochondrial [4Fe-4S] dependent lipoylation of dihydrolipoamide S-acetyltransferase (DLAT), and dihydrolipoamide S-succinyltransferase (DLST) [44, 47]. Knockdown of either ISCA1 or ISCA2 markedly decreased the lipoylation of DLAT and DLST in HeLa and 786-0 cells, whereas knockdown of IBA57 had minimal effects on lipoylation, confirming that both ISCA1 and ISCA2 play essential roles mitochondrial [4Fe-4S] protein assembly (S2D). Treatment of HeLa or 786-0 cells with #1 or #25, respectively, similarly inhibited the lipoylation of DLAT and DLST suggesting that these compounds also inhibit mitochondria [4Fe-4S] assembly (S2E) consistent with their functions as inhibitors of ISCA2. To determine whether knockdown of the other components of the L-ISC caused similar effects to ISCA2 on HIF regulation and iron sensing, we compared the effects of knockdown of each of the components of the L-ISC. The average decrease in target proteins after 6 days of siRNA transfection ranged between 50–95%, confirming that this method effectively decreased protein levels of ISCA1, ISCA2 and IBA57 (S3A). Intriguingly, we found that only knockdown of ISCA2 decreased levels of HIF-1α and HIF-2α, as well as IRP1, IRP2 and TFRC (Figs. 3A, S3A). We noted that ISCA1 levels were increased with ISCA2 siRNA whereas FTH1 levels appeared largely unchanged (Figs. 3A, S3A). Decreases in HIF-1/2α, IRP1 and FTH1 were observed after just 3-days' transfection with ISCA2 siRNA, which was associated with only 30% reduction in ISCA2 protein (S3B). The effects on ISCA2 knockdown on the HIFs were recapitulated using a different siRNA for ISCA2, showing that HIF-1α and HIF-2α levels were decreased as soon as 2 days post-transfection, when the decrease in ISCA2 protein was less apparent (Fig. 3B). We also observed a decrease in FTH1 with either of the two ISCA2 siRNAs at earlier time points that was not observed after 6 days' siRNA transfection, which may suggest dynamic regulation of FTH1 with ISCA2 loss that resembles that seen when cells were treated with #1 and #25 (Figs. 3B, S1E–F, 3B). The lack of effect of ISCA1 and IBA57 siRNA on the HIFs and IRPs was recapitulated using a second siRNA to these proteins (S3C). We also confirmed similar effects of ISCA2 knockdown in decreasing HIF-1/2α, IRP1, IRP2 and TFRC in RCC4 cells which are pVHL deficient, suggesting that ISCA2 plays a unique role in HIF regulation and iron sensing independently of its role in the L-ISC and independently of pVHL in multiple cell lines (Fig. 3C). Additionally, as seen with #1 and #25 (Fig. 1G), co-treatment of siRNA-transfected ACHN cells with MG132 did not prevent the loss of HIF-1/2α associated with ISCA2 knockdown (Fig. 3A) confirming that that observed decrease in HIF-1/2α occurred independently of the proteasome. Intriguingly, unlike that seen with #1 and #25, siRNA-mediated knockdown of ISCA1, ISCA2 and IBA57 significantly decreased *EPAS1* transcription but did not significantly affect *HIF1A* transcription (Fig. 3D). Since both ISCA1 and IBA57 knockdown decreased *EPAS1* transcript without affecting HIF-2α protein levels in ACHN cells, it is unlikely that the HIF-2α decrease mediated by ISCA2 siRNA is primarily due to decreased transcription. However, the decreased *EPAS1* transcription may be due to mitochondrial retrograde signaling in which dysfunctional mitochondria communicate with nuclear components, typically modulating transcription in response to mitochondrial stresses [48]. Using the SunSET assay, we found that ISCA2 knockdown abrogated the incorporation of puromycin into immunoprecipitated HIF2α, consistent with IRE-mediated inhibition of translation (Fig. 3E). We observed similar effects on of ISCA2 knockdown on HIF-1α translation, suggesting that ISCA2 may regulate HIF-1α translation through an unknown mechanism (Fig. 3E). When we investigated the impact of the ISC components on iron/metals content, we found that only ISCA2 knockdown induced marked elevation of total cellular iron and of other transition metals in ACHN and 786-0 cells (Figs. 3F, S3D). Taken together, our data suggest that ISCA2 knockdown or pharmacological inhibition decreases the translation of HIF-1α and HIF-2α and promotes metals accumulation through a mechanism that is independent of ISCA2's role in the L-ISC.

ISCA2 inhibition promotes cell death via ferroptosis

We noted that ISCA2 knockdown consistently decreased protein content to a greater extent than that observed with ISCA1 or IBA57 knockdown in a variety of cell lines (Fig. 4A). We also noted a consistent difference in media color indicating a higher pH in cells transfected with ISCA2 siRNA compared to those transfected with Con, ISCA1 or IBA57, which may reflect the strikingly lower cell density (and hence reduced metabolic activity) associated with ISCA2 knockdown (Fig. 4B, S4). In this regard, only ISCA1 knockdown promoted acidification of cell culture media, which likely reflects a defect in respiratory function (Fig. 4B) as previously reported [44]. Indeed, the profound reduction in the number of viable cells obtained with ISCA2 knockdown was confirmed using manual counting of trypan blue-excluding viable cells using two separate siRNAs (Fig. 4C). Cells transfected with ISCA2 siRNA also exhibited necrotic morphology such as cell enlargement and plasma membrane rupture, commonly observed in ferroptotic cells (S5) [49]. ISCA2 knockdown also significantly decreased the number of viable 786-0 cells compared to those transfected with Con siRNA, ISCA1 or IBA57 siRNA using the resazurin cell viability (Fig. 4D). Although no markers exist that can distinguish ferroptosis from other forms of programmed cell death, we used a kit that enables real-time monitoring of changes associated with cell death (Promega JA1011). We show that siRNA knockdown of ISCA2 resulted in induction of phosphatidyl serine (PS) on the cell surface, typically associated with early apoptosis, 24 h after siRNA transfection (Fig. 4E) followed by loss of membrane permeability, typically associated with secondary necrosis, 72 h after siRNA transfection (Fig. 4F). To further investigate ferroptosis as the mechanism of cell death induced by ISCA2 insufficiency, we utilized the ferroptosis inhibitor, liproxstatin, which is a radical-trapping antioxidant that slows the accumulation of lipid peroxides, thus blocking ferroptosis [50]. Co-treatment of cells with ISCA2 siRNA and liproxstatin significantly decreased cell death associated with ISCA2 knockdown (Fig. 5A), suggesting that ISCA2 knockdown induces cell death via ferroptosis. Similarly, treatment of 786-0 cells with #1 or #25 also decreased cell viability, which was attenuated by co-treatment with liproxstatin, the iron chelator, DFO, or the free radical scavenger N-acetyl cysteine (NAC), but not with the caspase inhibitor ZVAD-FMK, confirming that ISCA2 inhibition promotes death via ferroptosis (Fig. 5B, C). Like that seen with ISCA2 siRNA, treatment with #25 initially induced cell surface exposure of PS (S6Ai, left *Y*-axis), followed by loss of membrane permeability (Fig. S6Aii, right *Y*-axis), which was markedly attenuated by co-treatment with liproxstatin (S6Aii). We also noted that treatment with higher concentrations of #25 markedly decreased levels of GPX4 (S6B), which may sensitize cells to ferroptosis. #25 treatment also increased levels of the oxidized form of C11-BODIY (581/591), a fluorescent probe for indexing lipid peroxidation, confirming that #25 induces the lipid peroxidation associated with ferroptosis (Fig. 5D) [51]. Additionally, treatment with #25 but not with PT2385 (an analog of belzutifan) at concentrations expected to completely block HIF-2α activity (Figs. 1D, E, S6C) increased levels of malondialdehyde (MDA)-thiobarbituric (TBA) adducts, another indicator of lipid peroxidation, to a level comparable to the GPX4 inhibitor, RSL3, further confirming the ISCA2 inhibitors as inducers of lipid peroxidation

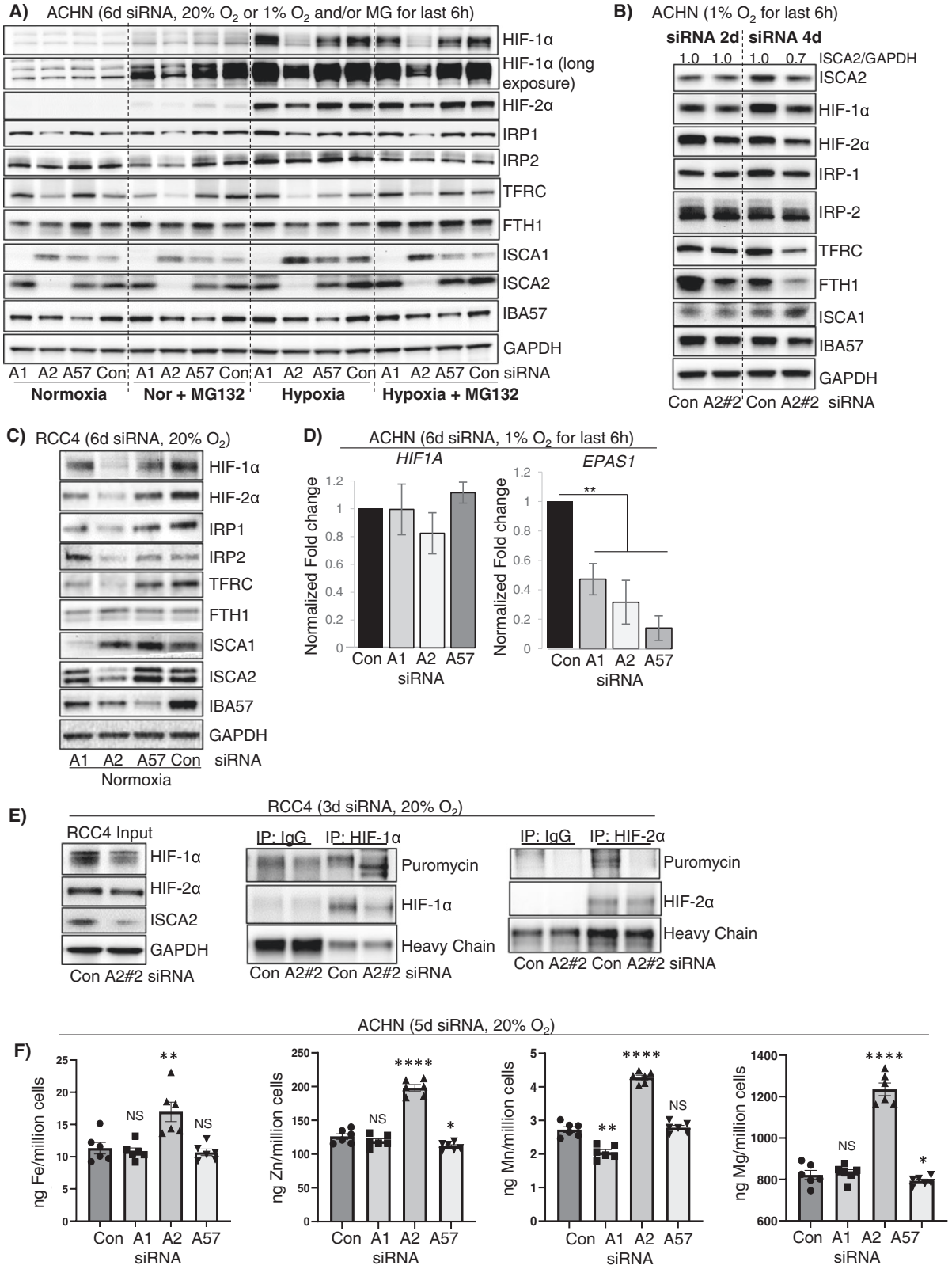

and downstream ferroptosis (Fig. 5E) [52]. Indeed, transmission electron microscopy of RCC10 cells treated with #25 show lost or irregular mitochondrial cristae and mitochondrial matrix with voids that are characteristic of ferroptosis (Fig. 5F) [53]. Taken together, the data suggests that ISCA2 inhibition promotes cell death via ferroptosis independently of its role in the ISC complex.

ISCA2 inhibition triggers synthetic lethality in pVHL deficient RCC cells

To investigate the relationship between ISCA2 and pVHL, we examined the effect of stable pVHL reconstitution in a panel of pVHL-deficient RCC cells. Strikingly, pVHL reconstitution resulted in marked upregulation of ISCA2 protein, whereas levels of ISCA1,

Fig. 3 ISCA2 depletion decreases HIF-1/2α levels and promotes iron and metals accumulation. A Western blots showing effect of 6-day siRNA knockdown of ISCA1 (A1), ISCA2 (A2), IBA57 (A57) or non-targeting siRNA (Con) in ACHN cells in 20% O_2 or after 6 h at 1% O_2 ± the proteasome inhibitor MG132 (5 μM and 1 μM for 6 h in 20% and 1% O_2 respectively). Densitometric analysis of ISCA2 band intensities normalized to GAPDH is shown in S3A. **B** Effect of 2- and 4-day knockdown of ISCA2 using a second ISCA2 siRNA construct (A#2) in ACHN cells in 1% O_2. Densitometric analysis of ISCA2 band intensities normalized to actin is shown above blots. **C** Effect of 6-day knockdown with indicated siRNAs in RCC4 cells. **D** Effect of transfection of indicated siRNAs on the transcription of *HIF1A* and *EPAS1* normalized to *B2M* in ACHN cells. **E** Effect of ISCA2 siRNA on HIF-1/2α translation in RCC4 cells. Cells were transfected with ISCA2 siRNA for 3 days, then labelled with puromycin. Puromycin incorporation was determined by immunoprecipitation of HIF-1/2α followed by western blot using an antibody against puromycin. **F** Effect of 5-day siRNA knockdowns on metals accumulation in ACHN cells detected using ICP-MS. Approximately equal cell numbers were submitted for analysis. All data are representative or averages of at least two independent experiments shown as mean ± SEM.

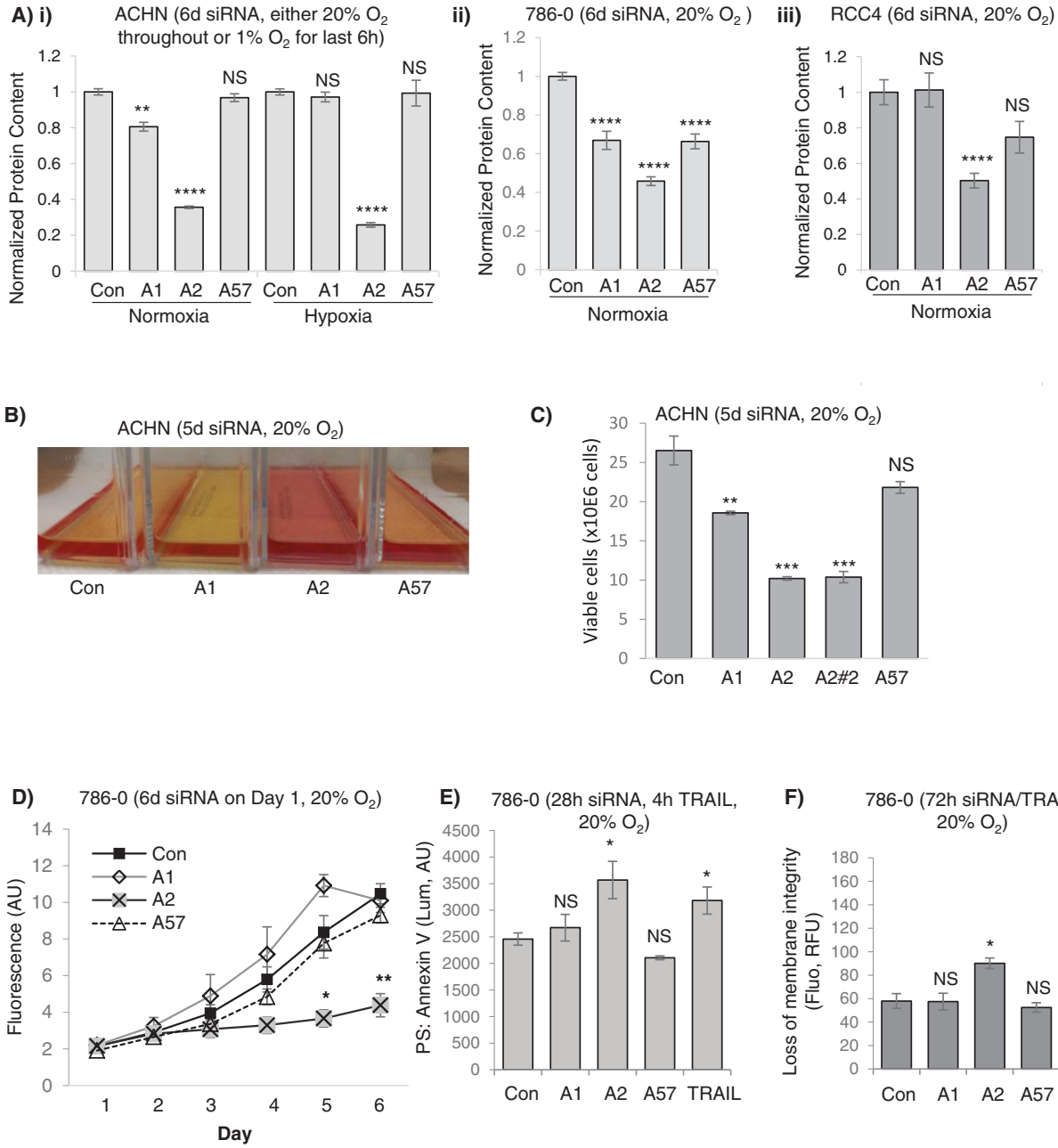

Fig. 4 SiRNA knockdown or pharmacological inhibition of ISCA2 induces cell death. A (i–iii) Effect of indicated siRNAs on total protein content in indicated cell lines (6 days post-transfection). **B** Media appearance of ACHN cells transfected with indicated siRNAs for 5 days. **C** Viable cell number determined by trypan blue exclusion in ACHN cells 5 days after transfection with indicated siRNAs. **D** Cell viability assay of 786-0 cells transfected with indicated siRNAs. Cells were seeded into 96-well plates 6 days after siRNA transfection, and cell viability was measured using resazurin daily for 6 days. **E** Effect of indicated siRNA on PS exposure in 786-0 cells 28 h after transfection. TRAIL (400 ng/ml, 4 h) is a positive control. **F** Effect of siRNA transfection in causing loss of membrane permeability in 786-0 cells 72 h after transfection using TRAIL (400 ng/ml, 72 h) as a positive control. Data shown are the mean ± SEM.

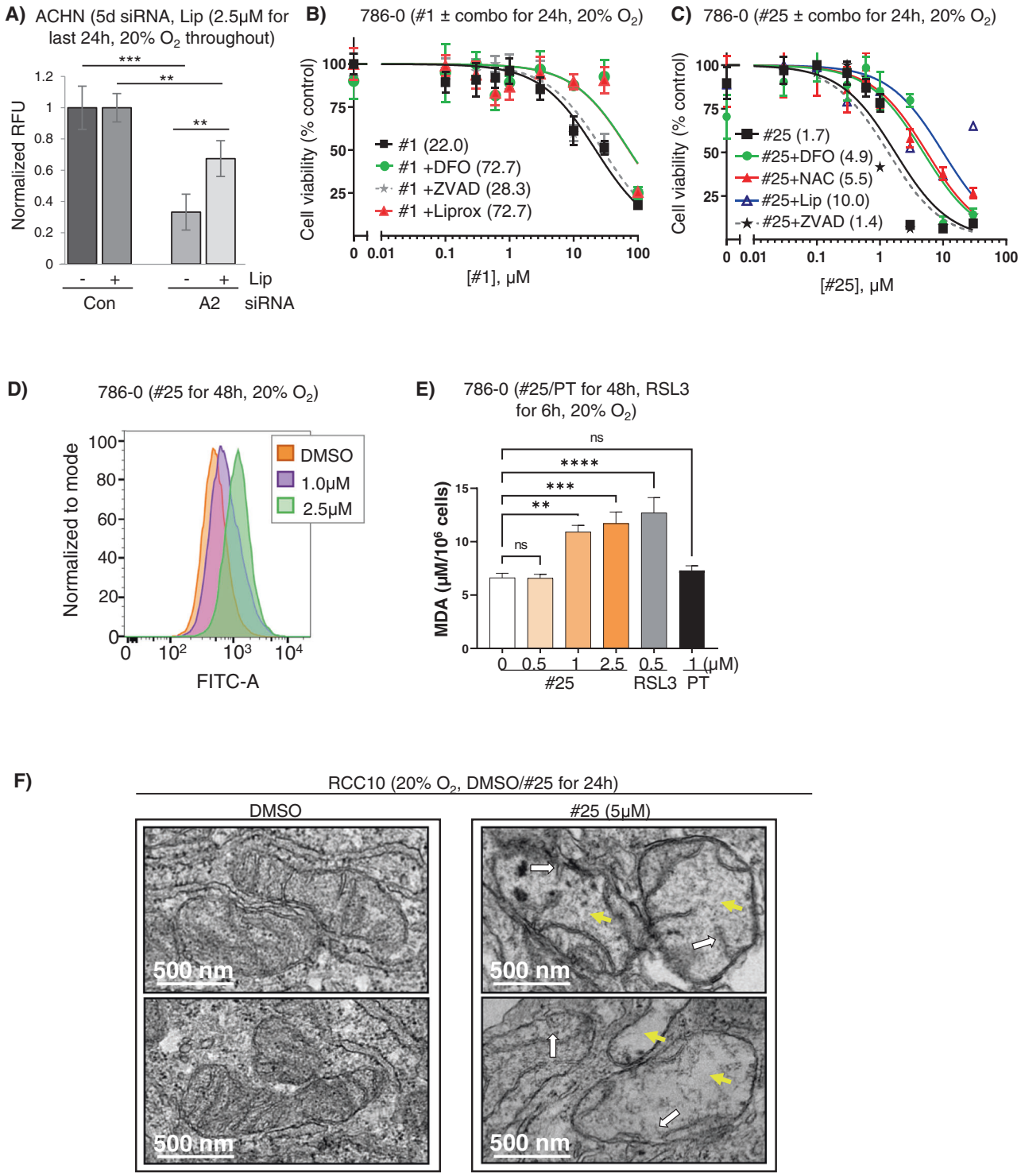

Fig. 5 ISCA2 inhibition induces ferroptosis. A Effect of co-treatment of ISCA2 siRNA and DMSO or liproxstatin (2.5 μM) on cell viability determined using resazurin in ACHN cells. siRNA transfection was performed for a total of 5 days with liproxstatin (or DMSO) added for the last 24 h. **B**, **C** Cell viability assays (resazurin) of 786-0 cells treated with (**B**) #1 or (**C**) #25, ± DFO (100 μM), liproxstatin (1 μM) or ZVAD-FMK (20 μM); or (**H**) #25 ± DFO (100 μM), NAC (1 mM), liproxstatin (1 μM) or ZVAD-FMK (20 μM). Treatments were performed for 24 h. Average IC_{50} values (μM) are shown in brackets. **D** Impact of #25 treatment (48 h) on BODIPY 581/591 fluorescence detected by flow cytometry in 786-0 cells. **E** Impact of 48 hours' treatment with #25, PT2385 (PT) or 6 hours' treatment with RSL3 on malondialdehyde (MDA), an indicator of lipid peroxidation in RCC10 cells. **F** Transmission electron microscopy of RCC10 cells treated with DMSO or #25 for 24 h (2 representative micrographs of each condition). DMSO-treated cells show normal mitochondria whereas #25-treated cells show damaged mitochondria including lost or irregular cristae (white arrows) and irregular matrix with voids (yellow arrows).

IBA57 and COX-IV did not show major changes (Fig. 6A), suggesting that the ISCA2 increase may not simply be a product of increased mitochondrial mass that is associated with pVHL re-expression [54–58]. Intriguingly, ISCA2 knockdown resulted in synthetic lethality in pVHL deficient 786-0 cells but not in 786-0 cells with pVHL reconstitution (Fig. 6B). pVHL reconstitution was also associated with 6- and 15-fold increases in resistance to #25 in RCC4 and 786-0 VHL cells compared to their parental pVHL deficient cells, respectively (Fig. 6C, D) with similar results seen with #1 (S6D). Consistent with this, stable ISCA2 overexpression promoted resistance to ISCA2 inhibition by #25 (Fig. 6E–G), and to ferroptosis induced by erastin (Fig. 6H) supporting the notion that cells with low ISCA2 are more sensitive to ISCA2 inhibition and to ferroptosis than those with high ISCA2. We noted that ISCA2 overexpression did not change the levels of HIF-1α or HIF-2α (Fig. 6E), nor the transcription of their target genes SLC2A1/*GLUT1* and *VEGFA* (S6E, F).

High ISCA2 is associated with better patient prognosis

To investigate the expression of ISCA2 in human tissue, we stained sections of ccRCC and uninvolved normal kidney for ISCA2. Analysis by board certified genitourinary pathologist (DS) revealed that ISCA2 staining in normal kidney exhibited a primarily diffuse cytosolic localization (which cannot be used to distinguish mitochondrial from cytosolic localization), with most intense staining within the epithelial cells of the proximal convoluted tubule (PCT, Fig. 7A). By contrast, ISCA2 staining was markedly lower in ccRCC tissue compared to uninvolved kidney possibly due to oncogenic transformation of PCT and resultant loss of structural integrity of organelles in which ISCA2 is found (Fig. 7A). Pathologist (DS) scoring of cores from uninvolved and tumor tissue from 19 patients with ccRCC showed a significance decrease in H-Score between ccRCC tissue compared to uninvolved kidney (Fig. 7B) confirming that ISCA2 levels are significantly lower in ccRCC than in normal kidney. To determine the relationship between ISCA2 levels and patient outcome, we investigated the association of ISCA2 protein levels and overall survival of in a cohort of 94 patients treated with anti-angiogenic tyrosine kinase inhibitors. Intriguingly, patients with ISCA2 levels above the median had significantly increased overall survival (hazard ratio high vs low ISCA2: 0.68; $p = 0.0197$; Fig. 7C) compared to those with ISCA2 levels below the median. We observed a similar association of high *ISCA2* transcript levels with better overall survival in TCGA-KIRC (Fig. 7D). Thus, the data suggest that low ISCA2 levels in ccRCC are associated with pVHL loss and with poorer prognosis, and that cells lacking functional pVHL are more sensitive to ISCA2 inhibition, in part due to decreased ISCA2. Taken together, the data suggest that the targeting of ISCA2 could be a strategy to inhibit HIF-α and induce ferroptosis particularly in pVHL deficient, more aggressive ccRCC cells.

ISCA2 inhibition significantly decreases tumor growth in vivo

To investigate the feasibility of ISCA2 inhibition as a therapeutic strategy for ccRCC, we used #25 as a probe compound based on its acceptable drug-like properties (bioavailability F = 27.3%; half-life $T_{1/2}$: 3.61 h, not shown). Oral administration of #25 once daily by oral administration resulted in a significant dose-dependent reduction of 786-0 tumor growth in vivo (Fig. 8A). Daily administration of #25 was well tolerated with no significant weight loss throughout the study (Fig. 8B). Treatment with 60 mg/kg #25 in RENCA syngeneic tumor xenografts also significantly inhibited tumor growth (Fig. 8C). This was accompanied by significantly decreased HIF-1α (HIF-2α levels were undetectable in the RENCA cells, Fig. S7) and in significantly elevated MDA (Fig. 8D, E). Thus, ISCA2 inhibition decreases HIF-α levels and induces the lipid peroxidation associated with ferroptosis both in vitro and in vivo and is a promising treatment strategy for ccRCC.

DISCUSSION

Proteins with Fe-S cofactors play important roles in fundamental cellular processes, including redox reactions, catalysis, protein translation, and DNA synthesis and repair [59]. The biogenesis of Fe/S proteins is catalyzed by complex, conserved assembly systems [43]. In eukaryotes including humans, Fe-S maturation is initiated in the mitochondria by the ISC machinery for the maturation of both mitochondrial and extra-mitochondrial Fe-S proteins [60]. ISCA1, ISCA2 and IBA57 play central roles in the later steps of mitochondrial [4Fe-4S] assembly, i.e. in the conversion of [2Fe-2S] clusters to [4Fe-4S] clusters for incorporation into mitochondrial [4Fe-4S] proteins, through a reaction that has not been well defined [44, 61]. Although ISCA1, ISCA2 and IBA57 form a ternary complex to convert two [2Fe-2S] clusters to a [4Fe-4S] cluster in *S. cerevisiae*, this ternary complex is not detected in human cells but instead, biophysical evidence suggest that the ISCA2-IBA57 complex coordinates the transfer of the [2Fe-2S] cluster from the core ISC to the ISCA2-ISCA1 complex for [4Fe-4S] assembly [61–65]. Strikingly, although all three were required for the proliferation of HeLa cells, only ISCA1 is essential for [4Fe-4S] assembly in non-dividing cells [44, 63].

In this study, through efforts to identify selective inhibitors for HIF-2α, we have identified compounds that not only inhibit HIF-2α but that also inhibit HIF-1α at higher concentrations. This greater potency of HIF-2α versus HIF-1α inhibition is an ideal combination for ccRCC since HIF-2α plays a central driving role in ccRCC progression and has limited expression in normal adult tissues, whereas HIF-1α, while also contributing to ccRCC progression, also plays a role in the homeostasis of some normal tissues [66]. Thus, by potently inhibiting HIF-2α and partially inhibiting HIF-1α, these compounds can be expected to exert maximal anti-tumor activity while maintaining a therapeutic window for minimal toxicity to normal tissue. Significantly, these compounds potently induce ferroptosis, which, by triggering a cytotoxic effect distinct from the cytostatic effects mediated by most other targeted therapies, will reduce the potential for the development of resistance [67]. Ferroptosis induction has attracted substantial attention as a therapeutic strategy in oncology since cancer cells that are resistant to conventional therapies or have a high propensity to metastasize are particularly susceptible to ferroptosis [68]. Ferroptosis induction is a particularly attractive therapeutic strategy for ccRCC since the metabolic reprogramming associated with pVHL loss that increases lipid storage and impairs fatty acid oxidation renders ccRCC cells exquisitely sensitive to ferroptosis induction [38, 69]. However, current ferroptosis inducers that are effective in vitro are unsuitable as clinical candidates since many target nodes that may be bypassed in vivo, or do not have suitable pharmacological properties for further clinical development [39, 40, 70]. Thus, the discovery of these ISCA2 inhibitors with the capacity to induce ferroptosis in vivo through oral administration provides a breakthrough for the in vivo induction of ferroptosis for the treatment of ccRCC and other solid tumor types. Taken together with their ability to inhibit HIF-1/2α, we anticipate that these ISCA2 inhibitors will elicit potent anti-tumor activity by blocking the tumor enabling functions of HIF1/2α both within tumor cells and within components of the tumor-permissive microenvironment, while inducing ferroptotic death selectively within pVHL-deficient tumor cells.

Our studies identify ISCA2 as an essential factor for the regulation of both HIF-1α and HIF-2α, and in the maintenance of iron homeostasis in renal cancer cells, and likely in other cancer cell types (S1A). We show that ISCA2 inhibition either pharmacologically or using siRNA blocks translation of both HIF-1α and HIF-2α, with greater potency of HIF-2α translational inhibition, by blocking IRE-dependent HIF-2α translation. The mechanism by which ISCA2 inhibition inhibits HIF-1α translation is unclear. However, it is likely that the impact of ISCA2 inhibition at least on HIF-2α translation is due to the triggering of the iron starvation response that promotes the binding of IRP1 to the HIF-2α IRE due

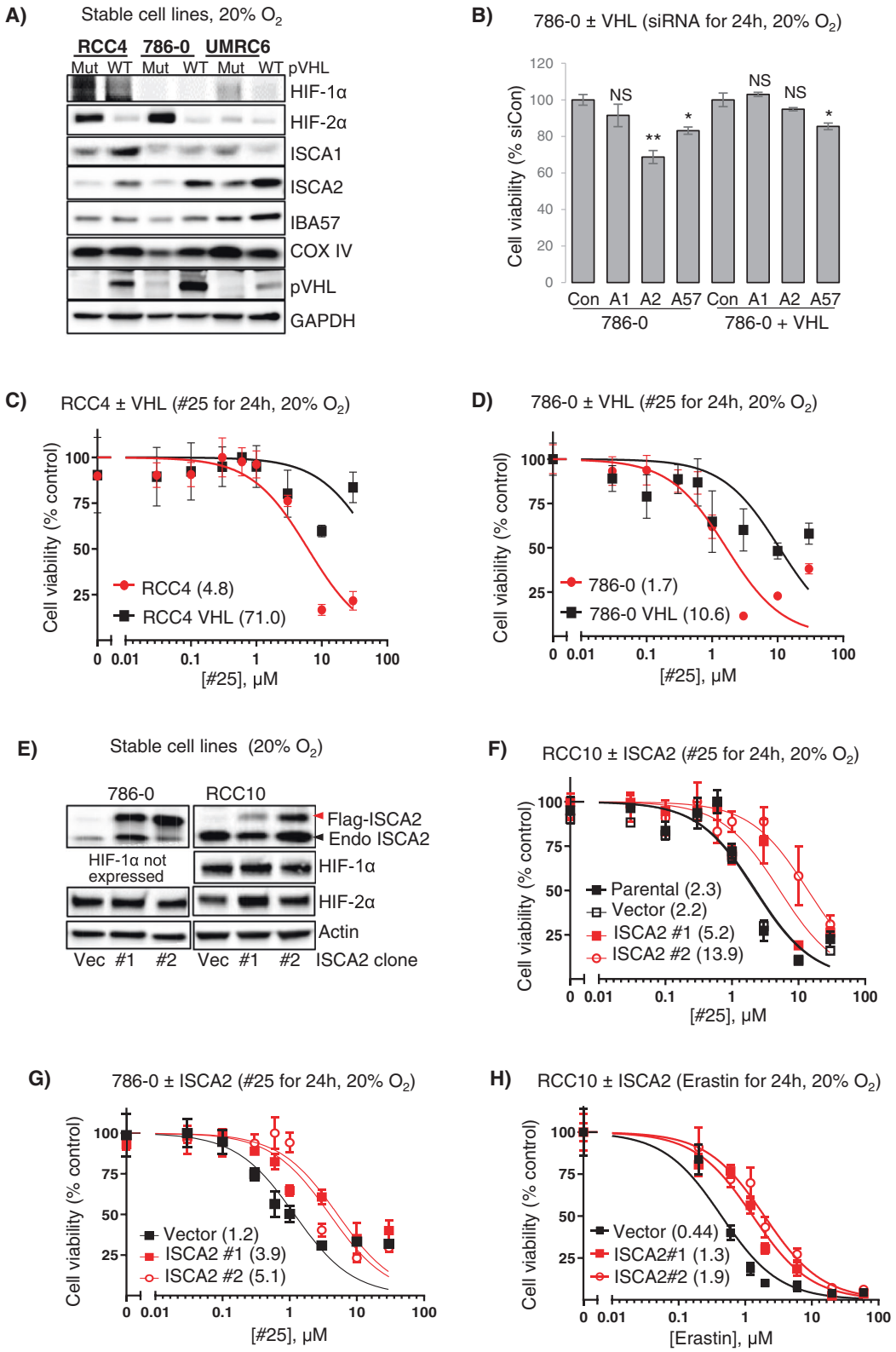

Fig. 6 VHL loss promotes sensitivity to ISCA2 inhibition. A ISCA2 levels in pVHL mutant ccRCC cells ± stable pVHL reconstitution. **B** Resazurin cell viability assay of 786-0 parental or 786-0 cells with pVHL reconstitution transfected with indicated siRNAs (24 h post-transfection). **C**, **D** Representative plot showing viability (resazurin) of RCC4 and RCC4 + VHL cells (**C**), and 786-0 and 786-0 +VHL cells (**D**), after treatment with #25 for 24 h. IC_{50} values (μM) are shown in brackets. **E** Western blots showing levels of endogenous (Endo) and overexpressed FLAG-ISCA2 in stable clones expressing empty vector (Vec) or ISCA2 from 786-0 and RCC10 cells (2 ISCA2 clones each). **F**, **G** Representative plots showing viability of RCC10 (**F**), or 786-0 (**G**) cells stably expressing empty vector (Vec) or ISCA2 treated with #25 for 24 h. IC_{50} values (μM) are shown in brackets. **H** Representative plots showing viability of RCC10 cells stably expressing empty vector (Vec) or ISCA2 treated with Erastin for 24 h. IC_{50} values (μM) are shown in brackets.

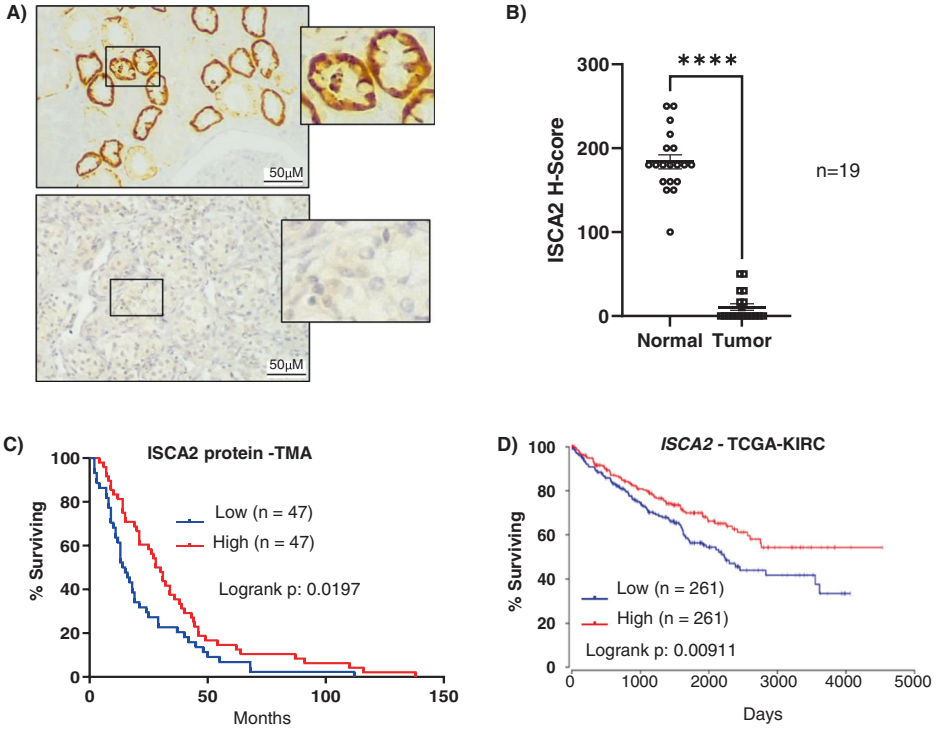

Fig. 7 ISCA2 is decreased in ccRCC and low ISCA2 is associated with poor patient prognosis. A Immunohistochemistry showing representative expression of ISCA2 in normal kidney (top) and in ccRCC (bottom). **B** Quantitation of ISCA2 H-Score in paired uninvolved and ccRCC cores from 19 patients. ****$p < 0.0001$ determined via Mann Whitney test. **C**, **D** Kaplan–Meier curves showing associations of (**C**) ISCA2 protein, or (**D**) *ISCA2* transcript levels above (high) or below (low) the median with overall survival using a tumor microarray (TMA; 94 cases) or data from TCGA-KIRC (522 cases) respectively.

to the loss of IRP1's Fe-S cluster [71]. The iron starvation response is clearly observed with pharmacological inhibition of ISCA2, which results in increased IRP2 and TFRC (which increase iron uptake) and decreased FTH1 (which decreases iron storage; Fig. 1E, F). These effects are less apparent with ISCA2 siRNA, possibly due to the increased duration of ISCA2 knockdown required for loss of ISCA2 protein, although shorter duration of ISCA2 knockdown results in loss of FTH1 and of HIF-1/2α suggesting that ISCA2 knockdown triggers the iron starvation response prior to when ISCA2 protein loss is apparent (Fig. 3B, S3B). Significantly, both pharmacological and siRNA-mediated ISCA2 knockdown is associated with significant accumulation of iron and of other transition metals (Figs. 2E–G, 3F, S2A–C, S3D). Thus, the decrease in IRP1, IRP2 and TFRC observed after prolonged knockdown of ISCA2 could be a response to this iron/metals accumulation (Figs. 2D, 3A). Of note, iron/metals accumulation was not observed when other components of the L-ISC, ISCA1 and IBA57 were knocked down, suggesting that ISCA2 possesses unique roles independent of its role in the L-ISC (Fig. 3F, S3D). Intriguingly, shRNA knockdown of NFS1, a sulfur donor in ISC biogenesis, also induces IRP2 and TFRC and depletes FTH1, sensitizing cells to ferroptosis (effects on HIF were not investigated) reminiscent of that seen in our current study [72]. Since NFS1 contributes to the maturation of both cytosolic and mitochondrial Fe-S proteins (unlike ISCA1, ISCA2 and IBA57 that are believed to contribute only to mitochondrial [4Fe-4S] assembly), our findings suggest that ISCA2 may play an earlier role in ISC assembly than previously thought [44, 73]. Our findings resemble that of a previous study that identified inhibitors of IRE-dependent HIF-2α translation using a screen in 786-0 cells [74]. Although the molecular target of these inhibitors was not identified (these inhibitors are structurally unrelated to the molecules described in our current study), the investigators also noted similar IRE-independent effects in inhibiting HIF-1α translation [74]. Taken together with our study, these findings suggests that HIF-1α translation may be iron regulated in an IRE-independent manner.

Our data suggest that inhibition of ISCA2 both decreases HIF-α levels and induces ferroptosis by triggering pathways that are independent of ISCA2's role in mitochondrial [4Fe-4S] assembly (Fig. 8F). We confirmed ferroptosis as the mechanism of cell death by the attenuation of cell death by co-treatment with the ferroptosis inhibitor, liproxstatin but not with the caspase (apoptosis) inhibitor, ZVAD-FMK (Fig. 5A–C) [50]. Furthermore, inhibition of ISCA2 was associated with profound changes in mitochondrial morphology (Fig. 5F) characteristic of ferroptotic cells [53] and resembles mitochondrial structural defects previously associated with ISCA2 deficiency [44]. ISCA2 levels are decreased with pVHL loss and patients with low ISCA2 levels have significantly decreased overall survival (Figs. 6A, 7C, D) suggesting that ISCA2 may play a tumor suppressor role. We note that since VHL status was not comprehensively evaluated in these patient datasets, the association between ISCA2 and VHL status could not be determined. Paradoxically, pVHL deficient cells with lower levels of ISCA2 are more sensitive to ferroptosis induced by ISCA2 inhibition and ISCA2 overexpression protected against death induced by ISCA2 inhibition and by the classical ferroptosis inducer, erastin (Fig. 6F–H). Taken together, the data suggest a therapeutic index for inducing cell death through ISCA2 inhibition specifically in pVHL deficient cells. Although the synthetic lethality of ISCA2 inhibition in pVHL deficient cells is serendipitous, IRP2 (*IREB2*) has been described as a valid VHL interactor, which may suggest a potential role of pVHL in the regulation of IRP2 and iron homeostasis [75]. Significantly, ISCA2 inhibition through oral administration significantly inhibits tumor growth and is well tolerated at the therapeutic dose (Fig. 8A–E), providing proof-of-concept for the efficacy and safety of ISCA2 inhibition for the treatment of ccRCC and other HIF driven and/or ferroptosis susceptible cancers.

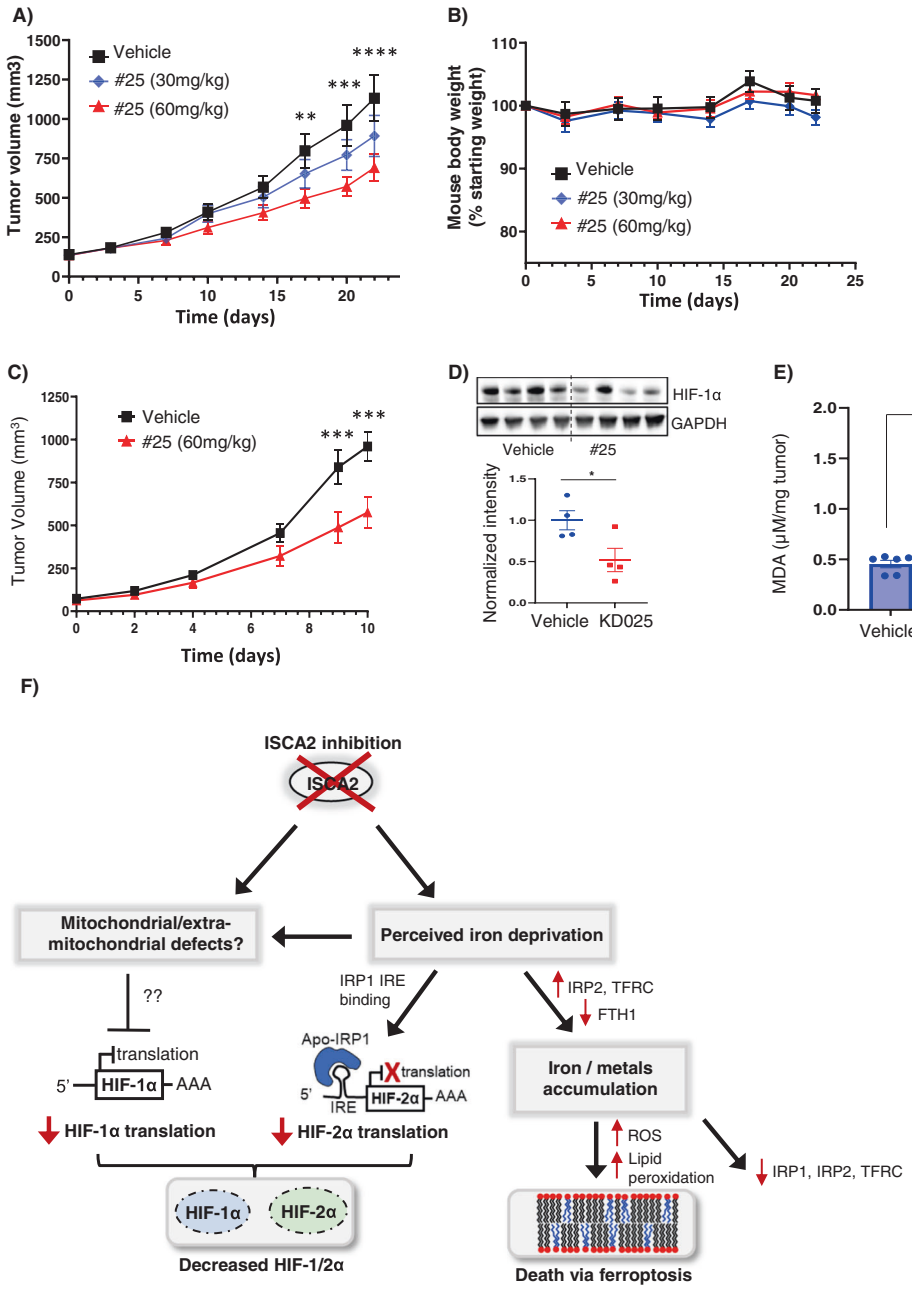

Fig. 8 ISCA2 inhibition inhibits xenograft growth in vivo. A, **B** Effect of treatment of 786-0 subcutaneous xenografts with vehicle or indicated doses of compound #25 (8 mice/group) administered orally once daily, on tumor volume (**A**), or mouse body weights (**B**). $^{**}p < 0.01$; $^{***}p < 0.001$; $^{****}p < 0.0001$ from Students' *T*-tests of vehicle versus 60 mg/kg treated group. p was not significant (NS) for 30 mg/kg treated group versus vehicle. **C** Effect of treatment of RENCA subcutaneous xenografts in syngeneic Balb/c mice with vehicle or 60 mg/kg #25 (8 mice/group) once daily. **D** Western blots showing HIF-1α and GAPDH with densitometric values normalized to GAPDH below. **E** MDA content of RENCA tumors from mice treated with vehicle or 60 mg/kg #25. **F** Proposed model for effects of ISCA2 blockade. Inhibition of ISCA2 using either small molecules or siRNA results in perceived iron deprivation, which induces upregulation of IRP2, TFRC and downregulation of FTH1, that together promote iron/metals accumulation that triggers cell death via ferroptosis, and also drives the later downregulation of IRP1, IRP2 and TFRC. This perceived iron deprivation also drives a shift to the IRE-binding form of IRP1 which inhibits HIF-2α translation. ISCA2 inhibition may also cause other mitochondrial/extramitochondrial defects dependent or independent of perceived iron deprivation that inhibits the translation of HIF-1α through unknown mechanisms. Thus, ISCA2 inhibition depletes both HIF-1α and HIF-2α and promotes cell death via ferroptosis.

MATERIALS AND METHODS

High throughput screen

The primary HTS was performed using 786-0 cells stably expressing HRE-Luciferase containing 5X copies of the HRE from the VEGFA in the pGL3 vector backbone. These cells were used to screen the MLPCN library of ~360,000 compounds at 18.8 μM in 1536-well format. Summary of the methods and results of the screen and counterscreens are described in Pubchem AIDs 624357, 624352, 652580, 652581 and 651589. Compound #1 was purchased from Molport (Beacon, NY) CAS ID: 862974-22-9, whereas #25 synthesis is described in is described in US patent 16/791148.

Cell lines and transfection reagents

ACHN, MIAPaCa-2 and 786-0 cells were from ATCC (Manassas, VA), whereas RCC4 and RCC10 cells were from M. Celeste Simon (University of Pennsylvania). All commercially available cell lines were authenticated

using STR fingerprinting upon receipt and stored in frozen aliquots. Fresh vials were thawed for use in experiments and discarded after 30–35 passages or approximately 2 months. Mycoplasma testing using the MycoAlert detection kit (Lonza, Ben OR) was performed every 2 months. Cells were maintained at 37 °C 5% CO_2 in Dulbecco's MEM (Life Technologies, ThermoFisher Scientific, Waltham MA) with 10% FBS. Hypoxia incubations were performed using a Whitley H35 Hypoxystation (HypOxygen, Frederick, MO). Lipofectamine™ RNAiMAX Transfection Reagent (ThermoFisher) was used for siRNA transfection. siRNAs were purchased from Dharmacon (Horizon Discovery, Lafayette CO) or Qiagen (Germantown, MD): siCon (Dharmacon D-001810-10), siCon#2 (Qiagen, #1022076), siISCA1 (Dharmacon L-014678-02), siISCA1#2 (Qiagen SI00434224) siISCA2#1 (Dharmacon L-019329-01), siISCA2#2 (Dharmacon L-019329-02), siIBA57 (Dharmacon L-021938-01), siIBA57#2 (Qiagen SI04195863).

Animal studies

6–8-week-old male NRG or Balb/c mice (10 per group) were injected subcutaneously with 10^7 786-0 cells or 2×10^6 RENCA cells respectively. When tumors became established, mice were stratified into groups of 8 mice approximately equal tumor sizes (average 150 mm^3 for 786-0 and 100 mm^3 for RENCA) and dosing was initiated. A sample size of 8 mice per group was selected to allow the detection of a 50% change of tumor burden with 80% power. Mice were dosed via PO daily with vehicle (0.5% methyl cellulose, 1% Tween 80) or indicated doses of #25 (HCL salt). Doses indicate concentrations of #25 free base. Tumor diameters were measured twice weekly at right angles (d_{short} and d_{long}) using electronic calipers and tumor volumes calculated by the formula volume = $(d_{short})^2 \times (d_{long})^2$ [76]. Studies were terminated when tumors reached 1000 mm^3. Although blinding of investigators to group allocation is an important component to decreasing bias in experimental design, due to limited personnel, investigators were not blinded to group allocations in this study. All animal studies were conducted in compliance with relevant local guidelines and were approved in the Institutional Animal Care and Use Committee.

TaqMan quantitative RT-PCR

Cell lysis and RNA extraction from siRNA transfected cells were performed using the RNeasy RNA extraction kit (Qiagen Inc, Germantown, MD). 1 µg of total RNA was reverse transcribed with the High-capacity RNA-to-cDNA kit (Applied Biosystems, Foster City, CA). For RT-PCR, cDNA was combined with TaqMan Gene Expression Mastermix (Applied Biosystems), and TaqMan primers for *B2M* (ThermoFisher, Hs00187842_m1), *HIF1A* (Hs00153153_m1), *EPAS1* (Hs01026149_m1), *POU5F1* (Hs03005111_g1) or *SOX2* (Hs04234836_s1). RT-PCR experiments were run on a QuantStudio 6 Flex System (Applied Biosystems). mRNA levels were calculated relative to the housekeeping gene, *B2M* using the ΔΔCt method as recommended by the manufacturer.

Immunoblotting

Western blotting was performed as previously described [77–79]. Antibodies for western blotting are listed in Supplementary Methods. Images were acquired using Fluorochem M imaging system (Protein Simple, San Jose, CA). Blot quantification was performed using multiplex band analysis provided by the AlphaView Software (Protein Simple).

Human subjects and ISCA2 IHC

Studies were conducted in accordance with the Declaration of Helsinki. Human ccRCC and uninvolved kidney tissue were obtained from archival samples from patients who had provided written informed consent according to protocols approval by the institutional review board at HCI. TMAs constructed from formalin fixed paraffin embedded treatment naïve tumor and uninvolved normal tissue from patients with advanced metastatic RCC that were later treated with antiangiogenic therapy. Samples were confirmed as ccRCC based on a combination of morphological, immunohistochemical and underlying genomic alterations. VHL status was evaluated only in a subset of tumors that were sequenced for clinical indication and indicated a VHL mutation rate of about 28% although other mechanisms of VHL loss (for example epigenetic mechanisms) are likely to be present. All specimens were reviewed by pathologists and representative tumor areas identified. Overall survival was defined as time from initiation of therapy until death. Three spatially separated 2 mm cores from archival FFPE tissue were included for each case. TMAs and tissue were stained for ISCA2 (HPA030492 Atlas antibodies, Bromma, Sweden) using conditions optimized using normal kidney according to the manufacturer's protocols using the BenchMark Ultra automated slide stainer (Ventana Medical Systems, Roche, Oro Valley, AZ). Manual pathologist quantitation in Fig. 7B was performed for uninvolved and ccRCC cores using the H-score quantitation, which is a product of intensity (1, 2 or 3+ for mild, moderate and strong) x the percentage of cells stained. Digital quantitation was performed for tumor tissue in Fig. 7C: Slides were scanned at 40X using a Leica Aperio AT2 scanner. Images were analyzed using Indica Labs HALO v2.3 TissueMicroArray module and CytoNuclear v1.6 algorithm customized for each stain type.

Statistical analysis

P-values, curve fitting and IC_{50} calculations, Kaplan Meier plots (with logrank *p*-values and hazard ratios) were determined using Prism Version 9.3.1 (GraphPad Software, San Diego). Where appropriate (i.e. data are normally distributed) differences between groups was determined using two-sided Students' *T*-tests using $p < 0.05$ as statistically significant. Mann–Whitney *U* tests were performed in Fig. 7B where ISCA2 H-score in tumor tissue were not normally distributed. Variance was similar between the groups being statistically compared. Analysis of *ISCA2* transcript levels from the 522 patient dataset from The Cancer Genome Atlas (TCGA) Kidney Renal Clear Cell Carcinoma (KIRC) database was performed by plotting Kaplan Meier Curves for the top and bottom 50 percentiles of *ISCA2* expression using OncoLnC [80].

Details on the DARTS, thermal shift, TEM and other assays as provided in Supplementary Data.

REFERENCES

1. Society AC Survival Rates for Kidney Cancer https://www.cancer.org/cancer/kidney-cancer/detection-diagnosis-staging/survival-rates.html Accessed 18 Mar 2022.
2. Gnarra JR, Tory K, Weng Y, Schmidt L, Wei MH, Li H, et al. Mutations of the VHL tumour suppressor gene in renal carcinoma. Nat Genet. 1994;7:85–90.
3. Moore LE, Nickerson ML, Brennan P, Toro JR, Jaeger E, Rinsky J, et al. Von Hippel-Lindau (VHL) inactivation in sporadic clear cell renal cancer: associations with germline VHL polymorphisms and etiologic risk factors. PLoS Genet. 2011;7:e1002312.
4. Banks RE, Tirukonda P, Taylor C, Hornigold N, Astuti D, Cohen D, et al. Genetic and epigenetic analysis of von Hippel-Lindau (VHL) gene alterations and relationship with clinical variables in sporadic renal cancer. Cancer Res. 2006;66:2000–11.
5. Ohh M, Park CW, Ivan M, Hoffman MA, Kim TY, Huang LE, et al. Ubiquitination of hypoxia-inducible factor requires direct binding to the beta-domain of the von Hippel-Lindau protein. Nat Cell Biol. 2000;2:423–7.
6. Wang GL, Jiang BH, Rue EA, Semenza GL. Hypoxia-inducible factor 1 is a basic-helix-loop-helix-PAS heterodimer regulated by cellular O2 tension. Proc Natl Acad Sci USA. 1995;92:5510–4.
7. Wilson WR, Hay MP. Targeting hypoxia in cancer therapy. Nat Rev Cancer. 2011;11:393–410. https://doi.org/10.1038/nrc3064.
8. An WG, Kanekal M, Simon MC, Maltepe E, Blagosklonny MV, Neckers LM. Stabilization of wild-type p53 by hypoxia-inducible factor 1alpha. Nature. 1998;392:405–8.
9. Ravi R, Mookerjee B, Bhujwalla ZM, Sutter CH, Artemov D, Zeng Q, et al. Regulation of tumor angiogenesis by p53-induced degradation of hypoxia-inducible factor 1alpha. Genes Dev. 2000;14:34–44.
10. Koshiji M, Kageyama Y, Pete EA, Horikawa I, Barrett JC, Huang LE. HIF-1alpha induces cell cycle arrest by functionally counteracting Myc. Embo J. 2004;23:1949–56.
11. Gustafsson MV, Zheng X, Pereira T, Gradin K, Jin S, Lundkvist J, et al. Hypoxia requires notch signaling to maintain the undifferentiated cell state. Dev Cell. 2005;9:617–28.
12. Choi H, Chun Y-S, Kim T-Y, Park J-W. HIF-2α enhances β-Catenin/TCF-Driven transcription by interacting with β-Catenin. Cancer Res. 2010;70:10101–11.
13. Bertout JA, Majmundar AJ, Gordan JD, Lam JC, Ditsworth D, Keith B, et al. HIF2{alpha} inhibition promotes p53 pathway activity, tumor cell death, and radiation responses. Proc Natl Acad Sci USA. 2009;106:14391–6.
14. Koh MY, Powis G. Passing the baton: the HIF switch. Trends Biochem Sci. 2012;37:364–72.
15. Cowman SJ, Fuja DG, Liu XD, Tidwell RSS, Kandula N, Sirohi D, et al. Macrophage HIF-1alpha is an Independent Prognostic Indicator in Kidney Cancer. Clin Cancer Res. 2020;26:4970–82.
16. Cowman SJ, Koh MY. Revisiting the HIF switch in the tumor and its immune microenvironment. Trends Cancer. 2022;8:28–42.

17. Hu CJ, Wang LY, Chodosh LA, Keith B, Simon MC. Differential roles of hypoxia-inducible factor 1alpha (HIF-1alpha) and HIF-2alpha in hypoxic gene regulation. Mol Cell Biol. 2003;23:9361–74.
18. Kapitsinou PP, Liu Q, Unger TL, Rha J, Davidoff O, Keith B, et al. Hepatic HIF-2 regulates erythropoietic responses to hypoxia in renal anemia. Blood 2010;116:3039–48.
19. Gruber M, Hu CJ, Johnson RS, Brown EJ, Keith B, Simon MC. Acute postnatal ablation of Hif-2alpha results in anemia. Proc Natl Acad Sci USA. 2007;104:2301–6.
20. Rankin EB, Biju MP, Liu Q, Unger TL, Rha J, Johnson RS, et al. Hypoxia-inducible factor-2 (HIF-2) regulates hepatic erythropoietin in vivo. J Clin Invest. 2007;117:1068–77.
21. Mastrogiannaki M, Matak P, Peyssonnaux C. The gut in iron homeostasis: role of HIF-2 under normal and pathological conditions. Blood 2013;122:885–92.
22. Sanchez M, Galy B, Muckenthaler MU, Hentze MW. Iron-regulatory proteins limit hypoxia-inducible factor-2alpha expression in iron deficiency. Nat Struct Mol Biol. 2007;14:420–6.
23. Raval RR, Lau KW, Tran MG, Sowter HM, Mandriota SJ, Li JL, et al. Contrasting properties of hypoxia-inducible factor 1 (HIF-1) and HIF-2 in von Hippel-Lindau-associated renal cell carcinoma. Mol Cell Biol. 2005;25:5675–86.
24. Kondo K, Kim WY, Lechpammer M, Kaelin WG Jr. Inhibition of HIF2alpha is sufficient to suppress pVHL-defective tumor growth. PLoS Biol. 2003;1:E83.
25. Dowd AA, Ibrahim FI, Mohammed MM. Renal cell carcinoma as a cause of iron deficiency anemia. Afr J Urol. 2014;20:25–7.
26. Vanharanta S, Shu W, Brenet F, Hakimi AA, Heguy A, Viale A, et al. Epigenetic expansion of VHL-HIF signal output drives multiorgan metastasis in renal cancer. Nat Med. 2013;19:50–6.
27. Micucci C, Matacchione G, Valli D, Orciari S, Catalano A. HIF2[alpha] is involved in the expansion of CXCR4-positive cancer stem-like cells in renal cell carcinoma. Br J Cancer (Mol Diagnostics). 2015;113:1178–85.
28. Bussolati B, Dekel B, Azzarone B, Camussi G. Human renal cancer stem cells. Cancer Lett. 2012;338:141–146.
29. Grange C, Tapparo M, Collino F, Vitillo L, Damasco C, Deregibus MC, et al. Microvesicles released from human renal cancer stem cells stimulate angiogenesis and formation of Lung Premetastatic Niche. Cancer Res. 2011;71:5346–56.
30. Covello KL, Kehler J, Yu H, Gordan JD, Arsham AM, Hu CJ, et al. HIF-2alpha regulates Oct-4: effects of hypoxia on stem cell function, embryonic development, and tumor growth. Genes Dev. 2006;20:557–70.
31. Li Z, Bao S, Wu Q, Wang H, Eyler C, Sathornsumetee S, et al. Hypoxia-inducible factors regulate tumorigenic capacity of glioma stem cells. Cancer Cell. 2009;15:501–13.
32. https://www.fda.gov/drugs/resources-information-approved-drugs/fda-approves-belzutifan-cancers-associated-von-hippel-lindau-disease Accessed 22 Mar 2022.
33. Choueiri TK, Bauer TM, Papadopoulos KP, Plimack ER, Merchan JR, McDermott DF, et al. Inhibition of hypoxia-inducible factor-2alpha in renal cell carcinoma with belzutifan: a phase 1 trial and biomarker analysis. Nat Med. 2021;27:802–5.
34. Gudas LJ, Fu L, Minton DR, Mongan NP, Nanus DM. The role of HIF1alpha in renal cell carcinoma tumorigenesis. J Mol Med (Berl). 2014;92:825–36.
35. Hoefflin R, Harlander S, Schafer S, Metzger P, Kuo F, Schonenberger D, et al. HIF-1alpha and HIF-2alpha differently regulate tumour development and inflammation of clear cell renal cell carcinoma in mice. Nat Commun. 2020;11:4111.
36. Dixon SJ, Lemberg KM, Lamprecht MR, Skouta R, Zaitsev EM, Gleason CE, et al. Ferroptosis: an iron-dependent form of nonapoptotic cell death. Cell 2012;149:1060–72.
37. Mou Y, Wang J, Wu J, He D, Zhang C, Duan C, et al. Ferroptosis, a new form of cell death: opportunities and challenges in cancer. J Hematol Oncol. 2019;12:34.
38. Zou Y, Palte MJ, Deik AA, Li H, Eaton JK, Wang W, et al. A GPX4-dependent cancer cell state underlies the clear-cell morphology and confers sensitivity to ferroptosis. Nat Commun. 2019;10:1617.
39. Yang WS, SriRamaratnam R, Welsch ME, Shimada K, Skouta R, Viswanathan VS, et al. Regulation of ferroptotic cancer cell death by GPX4. Cell 2014;156:317–31.
40. Zhang Y, Tan H, Daniels JD, Zandkarimi F, Liu H, Brown LM, et al. Imidazole Ketone Erastin Induces Ferroptosis and Slows Tumor Growth in a Mouse Lymphoma Model. Cell Chem Biol. 2019;26:623–33.
41. Schmidt EK, Clavarino G, Ceppi M, Pierre P. SUnSET, a nonradioactive method to monitor protein synthesis. Nat Methods. 2009;6:275–7.
42. Lomenick B, Jung G, Wohlschlegel JA, Huang J. Target identification using drug affinity responsive target stability (DARTS). Curr Protoc Chem Biol. 2011;3:163–80.
43. Lill R, Freibert SA. Mechanisms of Mitochondrial Iron-Sulfur Protein Biogenesis. Annu Rev Biochem. 2020;89:471–99.
44. Sheftel AD, Wilbrecht C, Stehling O, Niggemeyer B, Elsasser HP, Muhlenhoff U, et al. The human mitochondrial ISCA1, ISCA2, and IBA57 proteins are required for [4Fe-4S] protein maturation. Mol Biol Cell. 2012;23:1157–66.
45. Brancaccio D, Gallo A, Mikolajczyk M, Zovo K, Palumaa P, Novellino E, et al. Formation of [4Fe-4S] clusters in the mitochondrial iron-sulfur cluster assembly machinery. J Am Chem Soc. 2014;136:16240–50.
46. Wada K, Hasegawa Y, Gong Z, Minami Y, Fukuyama K, Takahashi Y. Crystal structure of Escherichia coli SufA involved in biosynthesis of iron-sulfur clusters: implications for a functional dimer. FEBS Lett. 2005;579:6543–8.
47. Schonauer MS, Kastaniotis AJ, Kursu VA, Hiltunen JK, Dieckmann CL. Lipoic acid synthesis and attachment in yeast mitochondria. J Biol Chem. 2009;284:23234–42.
48. Yang D, Kim J. Mitochondrial retrograde signalling and metabolic alterations in the tumour microenvironment. Cells 2019;22;8:275
49. Conrad M, Angeli JP, Vandenabeele P, Stockwell BR. Regulated necrosis: disease relevance and therapeutic opportunities. Nat Rev Drug Disco. 2016;15:348–66.
50. Zilka O, Shah R, Li B, Friedmann Angeli JP, Griesser M, Conrad M, et al. On the mechanism of cytoprotection by Ferrostatin-1 and Liproxstatin-1 and the role of lipid peroxidation in Ferroptotic cell death. ACS Cent Sci. 2017;3:232–43.
51. Pap EH, Drummen GP, Winter VJ, Kooij TW, Rijken P, Wirtz KW, et al. Ratio-fluorescence microscopy of lipid oxidation in living cells using C11-BODIPY(581/591). FEBS Lett. 1999;453:278–82.
52. De Leon JAD, Borges CR. Evaluation of oxidative stress in biological samples using the thiobarbituric acid reactive substances assay. J Vis Exp. 2020 May 12. https://doi.org/10.3791/61122
53. Hu CL, Nydes M, Shanley KL, Morales Pantoja IE, Howard TA, Bizzozero OA. Reduced expression of the ferroptosis inhibitor glutathione peroxidase-4 in multiple sclerosis and experimental autoimmune encephalomyelitis. J Neurochem. 2019;148:426–39.
54. Briston T, Stephen JM, Thomas LW, Esposito C, Chung YL, Syafruddin SE, et al. VHL-mediated regulation of CHCHD4 and mitochondrial function. Front Oncol. 2018;8:388.
55. Zhang H, Gao P, Fukuda R, Kumar G, Krishnamachary B, Zeller KI, et al. HIF-1 inhibits mitochondrial biogenesis and cellular respiration in VHL-deficient renal cell carcinoma by repression of C-MYC activity. Cancer Cell. 2007;11:407–20.
56. Hervouet E, Demont J, Pecina P, Vojtiskova A, Houstek J, Simonnet H, et al. A new role for the von Hippel-Lindau tumor suppressor protein: stimulation of mitochondrial oxidative phosphorylation complex biogenesis. Carcinogenesis 2005;26:531–9.
57. Hervouet E, Cizkova A, Demont J, Vojtiskova A, Pecina P, Franssen-van Hal NL, et al. HIF and reactive oxygen species regulate oxidative phosphorylation in cancer. Carcinogenesis 2008;29:1528–37.
58. Du W, Zhang L, Brett-Morris A, Aguila B, Kerner J, Hoppel CL, et al. HIF drives lipid deposition and cancer in ccRCC via repression of fatty acid metabolism. Nat Commun. 2017;8:1769.
59. Zanello P. Structure and electrochemistry of proteins harboring iron-sulfur clusters of different nuclearities. Part IV. Canonical, non-canonical and hybrid iron-sulfur proteins. J Struct Biol. 2019;205:103–20.
60. Paul VD, Lill R. Biogenesis of cytosolic and nuclear iron-sulfur proteins and their role in genome stability. Biochim Biophys Acta. 2015;1853:1528–39.
61. Muhlenhoff U, Richter N, Pines O, Pierik AJ, Lill R. Specialized function of yeast Isa1 and Isa2 proteins in the maturation of mitochondrial [4Fe-4S] proteins. J Biol Chem. 2011;286:41205–16.
62. Gelling C, Dawes IW, Richhardt N, Lill R, Muhlenhoff U. Mitochondrial Iba57p is required for Fe/S cluster formation on aconitase and activation of radical SAM enzymes. Mol Cell Biol. 2008;28:1851–61.
63. Beilschmidt LK, Ollagnier de Choudens S, Fournier M, Sanakis I, Hograindleur MA, Clemancey M, et al. ISCA1 is essential for mitochondrial Fe4S4 biogenesis in vivo. Nat Commun. 2017;8:15124.
64. Nasta V, Da Vela S, Gourdoupis S, Ciofi-Baffoni S, Svergun DI, Banci L. Structural properties of [2Fe-2S] ISCA2-IBA57: a complex of the mitochondrial iron-sulfur cluster assembly machinery. Sci Rep. 2019;9:18986.
65. Gourdoupis S, Nasta V, Calderone V, Ciofi-Baffoni S, Banci L. IBA57 Recruits ISCA2 to Form a [2Fe-2S] Cluster-Mediated Complex. J Am Chem Soc. 2018;140:14401–12.
66. Kumar T, Pandey R, Chauhan NS. Hypoxia Inducible Factor-1alpha: The Curator of Gut Homeostasis. Front Cell Infect Microbiol. 2020;10:227.
67. Rini BI, Atkins MB. Resistance to targeted therapy in renal-cell carcinoma. Lancet Oncol. 2009;10:992–1000.
68. Chen X, Kang R, Kroemer G, Tang D. Broadening horizons: the role of ferroptosis in cancer. Nat Rev Clin Oncol. 2021;18:280–96.
69. Miess H, Dankworth B, Gouw AM, Rosenfeldt M, Schmitz W, Jiang M, et al. The glutathione redox system is essential to prevent ferroptosis caused by impaired lipid metabolism in clear cell renal cell carcinoma. Oncogene 2018;37:5435–50.
70. Schneider M, Wortmann M, Mandal PK, Arpornchayanon W, Jannasch K, Alves F, et al. Absence of glutathione peroxidase 4 affects tumor angiogenesis through increased 12/15-lipoxygenase activity. Neoplasia 2010;12:254–63.
71. Hirling H, Henderson BR, Kuhn LC. Mutational analysis of the [4Fe-4S]-cluster converting iron regulatory factor from its RNA-binding form to cytoplasmic aconitase. EMBO J. 1994;13:453–61.
72. Terzi EM, Sviderskiy VO, Alvarez SW, Whiten GC, Possemato R. Iron-sulfur cluster deficiency can be sensed by IRP2 and regulates iron homeostasis and sensitivity to ferroptosis independent of IRP1 and FBXL5. Sci Adv. 2021;7:eabg4302

73. Biederbick A, Stehling O, Rosser R, Niggemeyer B, Nakai Y, Elsasser HP, et al. Role of human mitochondrial Nfs1 in cytosolic iron-sulfur protein biogenesis and iron regulation. Mol Cell Biol. 2006;26:5675–87.
74. Zimmer M, Ebert BL, Neil C, Brenner K, Papaioannou I, Melas A, et al. Small-molecule inhibitors of HIF-2a translation link its 5'UTR iron-responsive element to oxygen sensing. Mol Cell. 2008;32:838–48.
75. Wang J, Pantopoulos K. The pathway for IRP2 degradation involving 2-oxoglutarate-dependent oxygenase(s) does not require the E3 ubiquitin ligase activity of pVHL. Biochim Biophys Acta. 2005;1743:79–85.
76. Paine-Murrieta GD, Taylor CW, Curtis RA, Lopez MH, Dorr RT, Johnson CS, et al. Human tumor models in the severe combined immune deficient (scid) mouse. Cancer Chemother Pharm. 1997;40:209–14.
77. Koh MY, Darnay BG, Powis G. Hypoxia-associated factor, a novel E3-ubiquitin ligase, binds and ubiquitinates hypoxia-inducible factor 1alpha, leading to its oxygen-independent degradation. Mol Cell Biol. 2008;28:7081–95.
78. Koh MY, Lemos R Jr, Liu X, Powis G. The Hypoxia-Associated Factor Switches Cells from HIF-1{alpha}- to HIF-2{alpha}-Dependent Signaling Promoting Stem Cell Characteristics, Aggressive Tumor Growth and Invasion. Cancer Res. 2011;71:4015–27.
79. Koh MY, Nguyen V, Lemos R, Darnay BG, Kiriakova G, Abdelmelek M, et al. Hypoxia-Induced SUMOylation of E3 Ligase HAF Determines Specific Activation of HIF2 in Clear-Cell Renal Cell Carcinoma. Cancer Res. 2015;75:316–29.
80. Anaya J. OncoLnc: linking TCGA survival data to mRNAs, miRNAs, and lncRNAs. PeerJ Computer Sci. 2016;2:e67.

ACKNOWLEDGEMENTS

We acknowledge technical support by Linda Nikolova for the TEM studies.

AUTHOR CONTRIBUTIONS

YSG designed and performed experiments, interpreted data and contributed intellectually to the writing of the manuscript. MCFDS, DGF and ECR designed and performed experiments and interpreted data. ARC performed the mass spectrometry for the DARTS assay and contributed to experimental design and data analysis. SJC and KAP performed additional cell viability studies and performed data analysis whereas JK and SRT optimized and performed digital quantitation of the immunohistochemistry for ISCA2. EAL provided critical feedback for the preparation of the manuscript. DS and NA contributed to the preparation of the tumor microarray whereas DS provided H-Scores for ISCA2 expression. XL designed and optimized the ISCA2 inhibitors. MYK conceived of the project, performed DARTS and thermal shift experiments and wrote the manuscript.

FUNDING

This work was supported by NIH grants R03DA033980, CA181106 and CA217905 and Dod KCRP grant KC190022 to MYK, NIH grant R43 CA217385-A1 to XL, and NIH Hematology Training Program Grant T32DK007115 to DF. We acknowledge financial support by the Huntsman Cancer Foundation. Research reported in this publication utilized the Preclinical Research Shared Resource at Huntsman Cancer Institute at the University of Utah. The content is solely the responsibility of the authors and does not necessarily represent the official views of the NIH.

COMPETING INTERESTS

MYK is founder and has equity in Kuda Therapeutics Inc. All other authors declare no conflict of interest.

ADDITIONAL INFORMATION

Supplementary information The online version contains supplementary material available at https://doi.org/10.1038/s41388-022-02460-1.

Correspondence and requests for materials should be addressed to Mei Yee Koh.

Reprints and permission information is available at http://www.nature.com/reprints

Publisher's note Springer Nature remains neutral with regard to jurisdictional claims in published maps and institutional affiliations.